Molecular Structure and Thermal Behavior of Poly(methyl methacrylate) Thermoreversible Gels and Aggregates

Nazir Fazel,[†,‡] Annie Brûlet,[§] and Jean-Michel Guenet*[,†]

Laboratoire d'Ultrasons et de Dynamique des Fluides Complexes, Université Louis Pasteur, CNRS URA 851, 4 rue Blaise Pascal, F-67070 Strasbourg Cedex, France, Laboratoire de Physique des Liquides et Interfaces, Université de Metz, F-57070 Metz Cedex, France, and Laboratoire Léon Brillouin, CEA-CNRS, CEN Saclay, F-91191 Gif-sur-Yvette Cedex, France

Received December 3, 1993; Revised Manuscript Received March 21, 1994[⊗]

ABSTRACT: The formation of thermoreversible gels and aggregates of poly(methyl methacrylate) (PMMA) has been investigated as a function of temperature in two different solvents, i.e., bromobenzene and *o*-xylene. The molecular structure and the thermal behavior have been determined and correlated. It is again shown that the systems are composed of rigid, interconnected cylinders characterized by a two-population distribution as far as the transverse cylinder radius, r_H, is concerned: a majority of cylinders with $r_H = 1.5 \pm 0.1$ nm and a minority of cylinders with $r_H = 3.5$–4.0 nm. When the gelation sets in, the proportion of the second population is seen to increase substantially at the expense of the first population. These results are interpreted with a *fringed-micelle* model in which the physical junctions consist of the large-radius population of cylinders. The results and conclusions are discussed in the light of a solvated double-helical conformation.

Introduction

The thermoreversible gelation of poly(methyl methacrylate) (PMMA) displays some interesting features that make this system a kind of hybrid between synthetic polymers and biopolymers. As synthetic polymers, PMMA gels form in a large variety of organic solvents.[1-3] As biopolymers, stereoregular PMMAs possess the ability to form double helices.[4,5] Even mixtures of syndiotactic PMMA (sPMMA) and isotactic PMMA (iPMMA) can form a double-helical structure, called a stereocomplex, in which the syndiotactic chain wraps around the isotactic filament.[6]

Recently, we reported on a study of the molecular structure and the rheological behavior of such gels.[7,8] This investigation revealed that PMMA gels consisted of an array of rigid rods connected to one another (these results were obtained with the same PMMA sample used in this study). In these papers, we also came to the conclusion that the junctions were probably disorganized (*flail-like model*) as opposed to rigid, organized junctions (*bunch-like model*). Both are *fringed-micelle models*, a structure already put forward by Schomaker and Challa in the case of stereocomplex associations.[9,10] Here, we report on a new study of these system as a function of temperature by small-angle neutron scattering and thermal analysis. This study leads us to reconsider our former interpretation as to the junction structure. While we confirm the existence of a rod-like basic structure of radius 1.5 ± 0.1 nm, the new evidences are not consistent with the *flail-like model*. On the contrary, the body of experimental results suggests far better agreement with the *bunch-like model*. These conclusions meet those drawn recently on κ-carrageenans.[11] The thermal behavior observed during gel formation together with the neutron scattering data gives further evidence that the gel mechanism proceeds via two steps:[12,13] first *helix formation* and second *helix aggregation*.

* To whom correspondence should be addressed.
† Laboratoire d'Ultrasons et de Dynamique des Fluides Complexes, Université Louis Pasteur, CNRS URA 851.
‡ Laboratoire de Physique des Liquides et Interfaces, Université de Metz.
§ Laboratoire Léon Brillouin, CEA-CNRS.
⊗ Abstract published in *Advance ACS Abstracts*, May 15, 1994.

Experimental Section

(1) Materials. The polymethacrylate sample used in this study was supplied by Röhm GmbH (Germany). Its weight-average molecular weight and polydispersity index were determined by size exclusion chromatography in THF at 25 °C. The following values were obtained: $M_w = 1.05 \times 10^5$; $M_w/M_n \approx 2.86$. Tacticity was evaluated from the triad population by ^{1}H NMR in deuterated chloroform. The proportions of iso, syndio, and hetero triads are as follows: i = 18%, h = 15%, and s = 67%. It is worth mentioning that the polymer sample used in this study is the same one as previously studied (sPMMA1).[7,8]

For the small-angle neutron scattering experiments deuterated solvents were used: *o*-xylene and bromobenzene purchased from Aldrich (99% deuteration). For the thermal analysis the protonated counterparts from the same supplier were used.

(2) Sample Preparation. Depending upon the solvent one or two polymer concentrations were investigated: in bromobenzene 0.03 and 0.17 g/cm^3 and in *o*-xylene 0.03 g/cm^3. In what follows these concentrations will be designated as 3% and 17%, respectively.

The sample for neutron scattering experiments was directly prepared in a sealable quartz cell by weighing the appropriate amounts of polymer and solvent. Once sealed, homogeneous solutions were obtained by heating close to the solvent's boiling point. Gels were formed by quenching at the desired temperature.

The sample for DSC experiments was first prepared in a test tube and then gelled at 0 °C for a minimum of 1 h. Pieces of gel were cut off and rapidly transferred into "volatile" sample pans (inox pans) which were hermetically sealed. These pans contained approximately 100 μL of gel. Before any measurements the system was reinitialized by heating to 150 °C with subsequent isothermal annealing at that temperature.

(3) Thermal Analysis. Thermograms of gel melting or gel formation were determined on a Mettler DSC30 equipped with a high-sensitivity detection head. Liquid nitrogen was used as a coolant. Heating and cooling rates of 2, 1, 0.5, and 0.25 °C/min were employed. A sample pan containing an equivalent amount of solvent was used as a reference cell to compensate for thermal inertia arising from the use of large quantities of gel. Spectra were processed as usual. The intrinsic electronic noise of the apparatus was reduced by using smoothing procedures.

(4) Small-Angle Neutron Scattering. The experiments were carried out on PAXE and PAXY cameras located at the Laboratoire Léon Brillouin (LLB) (CEN Saclay, France). With both cameras a wavelength of $\lambda = 0.6$ nm was used with a wavelength distribution characterized by a width at half-height $\Delta\lambda/\lambda_m \approx 10\%$. The cameras possess a two-dimensional counter composed of 64 × 64 cells for PAXE and 128 × 128 detection cells for PAXY (further details are available on request at LLB).

0024-9297/94/2227-3836$04.50/0

By varying the sample–detector distance the investigated q range was $0.1 < q\ (nm^{-1}) < 2.5$, with $q = (4\pi/\lambda)\sin(\theta/2)$ where θ is the scattering angle.

Counter normalization was achieved by using an incoherent spectrum scattered by a 1-mm-thick hydrogenated decalin sample.

As hydrogenated polymers were used, their incoherent signal had to be accounted for and removed from the total signal to obtain only the coherent intensity. The usual procedure is to use a blank sample composed of the deuterated solvent plus an appropriate amount of a small protonated molecule which mimics the polymer unit. Obviously, the mixture must be homogeneous; that is, it must behave ideally. While this procedure usually works for $q < 1.3$ nm, because the signal is much larger than the background, for larger q the background may become significantly larger than the signal, particularly for high polymer concentrations. This arises from the fact that the blank sample also scatters an additional coherent signal due to the contrast between the solvent and the host small molecule. The blank I_0 should be

$$I_0 = I_{sol}^{coh} + I_{inc} \tag{1}$$

in which I_{sol}^{coh} is the solvent coherent intensity ($I_{sol}^{coh} = b_{sol}^2 k_B T \chi$) and I_{inc} is the polymer incoherent intensity (the incoherent intensity from the deuterated solvent, being much lower than that of hydrogen, is ignored here). Instead, in a dilute mixture of a protonated molecule within a deuterated solvent displaying ideal behavior, one measures[14]

$$I_0 = \phi k_B T \chi_T \frac{b_{sol}^2}{v_{sol}} + I_{inc} + k_B T \frac{\phi(1-\phi)v_H^2}{v_{sol}^2}[b_{sol} - (v_{sol}/v_H)b_H]^2 \tag{2}$$

in which ϕ is the volume fraction of the deuterated solvent. The third term can be as important as I_{inc}, especially when the concentration of the protonated species is increased.

As the additional coherent term is not straightforwardly evaluated, we considered two blanks for the 3% systems. The upper one, I_{up}, was obtained with a sample containing the solvent plus a given quantity of 2,4-pentanedione ($C_5H_8O_2$, which mimics the PMMA unit):

$$I_{up} = \frac{I_M - (T_M/T_e)I_e}{\delta_M[I_d - (T_d/T_e)I_e]} \tag{3}$$

in which I_M, I_d, and I_e are the intensities scattered by the mixture, decalin, and the empty cell, respectively, T, with the appropriate subscripts, their transmissions, and δ_M the sample's thickness.

The second one, I_{low}, was calculated from the spectrum of the pure solvent to which is added the calculated incoherent signal of the polymer. The latter was calculated by assuming the incoherent scattering to be directly proportional to the number of moles of protons per unit molar volume, N_p/V_m, for the mixture of *protonated polymer in the deuterated solvent*. The direct proportionality between N_p/V_m and I_{inc} was checked on several protonated solvents (see Figure 1 and the corresponding caption). This allows one to establish an experimental variation of I_{inc} (normalized to decalin, transmission, and thickness) as a function of N_p/V_m:

$$I_{inc} = \frac{I_H - (T_H/T_e)I_e}{I_d - (T_d/T_e)I_e} = 8.65 N_p/V_m \tag{4}$$

in which I_H and T_H are the intensity scattered by the hydrogenated solvent and its transmission, respectively.

I_{low} was then calculated from

$$I_{low} = \frac{I_{sol}^{coh} - (T_{sol}/T_e)I_e}{T_{sol}\delta_{sol}(I_d/T_d - I_e/T_e)}(1 - \phi_{pol}) + 8.65\phi_{pol}N_{p_{pol}}/V_{m_{pol}} \tag{5}$$

in which ϕ_{pol} is the polymer volume fraction and I_{sol}^{coh} is the intensity scattered by the deuterated solvent with T_{sol} and δ_{sol} the corresponding transmission and thickness.

The blank used was accordingly

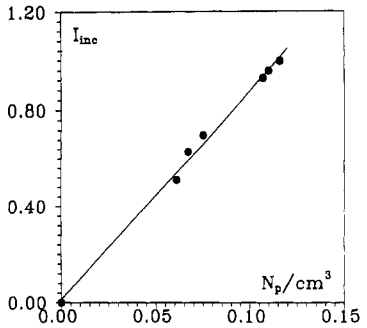

Figure 1. Incoherent intensity scattered by 1-mm-thick samples as a function of the number of protons per cm^3 (number of protons of the molecule/molar volume): from top to bottom, decalin, octane, hexane, toluene, benzene, and 1,2-dichloropropane. Concerning toluene, benzene, and 1,2-dichloropropane, there is an additional coherent scattering, which is, however, negligible compared to the incoherent scattering and which can be ignored.

$$I_0 = (I_{up} + I_{low})/2 \tag{6}$$

The resulting polymer coherent intensity was finally bracketed with error bars whose upper and lower values were calculated by using I_{up} and I_{low} as background, respectively. Concerning the 17% system, for which the background becomes slightly larger than the signal at very high q ($q > 0.2$ nm^{-1}), the value of I_{up} was determined by taking the value of the intensity scattered by the gel at the highest q value.

The coherent, normalized intensity scattered by the sample, $I_N(q)$, was finally derived from

$$I_N(q) = \frac{\frac{I_s(q)}{T_s\delta_s}}{\frac{I_d(q)}{T_d} - \frac{I_e(q)}{T_e}} - I_0 \tag{7}$$

in which $I_s(q)$ is the coherent intensity scattered by the sample, and T_s and δ_s are its transmission and thickness.

The absolute intensity scattered by the polymer of concentration C_p is

$$I_A(q) = \frac{I_N(q)}{K} = C_p S_p(q) \tag{8}$$

in which K reads

$$K = \frac{(b_p - y_{ps}b_{sol})^2(4\pi)\delta_d N_A T_d}{g(\lambda_m)(1 - T_d)m_p^2} \tag{9}$$

in which b_p and b_{sol} are the scattering amplitudes of the polymer and the solvent, respectively, y_{ps} is the ratio of the polymer molar volume to the solvent molar volume, m_p is the polymeric unit molecular weight, and $g(\lambda_m)$ is a correction factor which depends upon the neutron wavelength λ_m and the camera.[15] In the present case, this correction factor has been determined by Cotton's method.[16]

Results and Discussion

(1) PMMA/Bromobenzene Gels and Aggregates. The effect of quenching temperature was studied on 3% systems. Typically, the system was first molten at 150 °C (close to bromobenzene's boiling point) and then cooled rapidly to the desired temperature at which it was held for a minimum of 3 h prior to any neutron scattering measurements. Four temperatures were investigated: 92, 70, 45, and 20 °C. At 45 °C and above, the system did not gel whereas it did at 20 °C.

Results for the four temperatures are reported in Figure 2 by means of a Kratky representation. As can be seen, the intensity for the sample prepared at 20 °C is by far

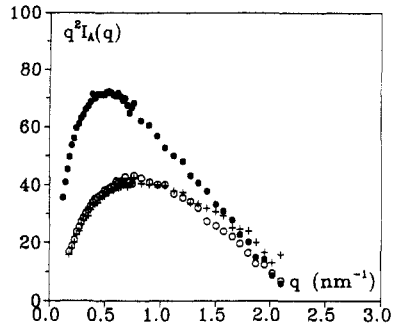

Figure 2. Kratky plot ($q^2I(q)$ vs q) of the intensity scattered by 3% systems in bromobenzene at different quenching temperatures: (●) 20 °C; (○) 45 °C; (+) 90 °C.

the highest one, which is consistent with the occurrence of gelation in this sample.

As with previous results,[8] the data shown here can be fitted with a relation derived for a population of cylinders of infinite length and radius r_{Hi}. This relation assumes that the intensity is simply the superposition of the intensity scattered by each cylinder provided that $l_n \gg r_{Hi}$, where l_n is the network mesh size:

$$q^2I_A(q) = C_p\left[\pi q\sum_i w_i\mu_{Li}\frac{4J_1^2(qr_{Hi})}{(qr_{Hi})^2} + \text{const}\right] \quad (10)$$

in which J_1 is the Bessel function of the first kind and first order and w_i is the weight fraction of cylinders with radius r_{Hi} and mass per unit length μ_{Li}. The constant term is proportional to the number per unit volume of crossing between cylinders and of kinks.

If the constant term is either negligible or properly subtracted—which gives $I_{A0}(q)$—then one may plot the results in the range $qr_{Hi} < 1$ by means of a Porod plot:

$$\log[qI_{A0}(q)] = \log C_p\pi\sum_i w_i\mu_{Li} - \frac{q^2}{4}\frac{\sum_i w_i\mu_{Li}r_{Hi}^2}{\sum_i w_i\mu_{Li}} \quad (11)$$

The average radius $\langle r_H^2\rangle$ is accordingly

$$\langle r_H^2\rangle = \frac{\sum_i w_i\mu_{Li}r_{Hi}^2}{\sum_i w_i\mu_{Li}} \quad (12)$$

A typical Porod plot is given in Figure 3 for the 45 °C system. As expected, a linear variation is obtained which gives $\langle r_H^2\rangle^{1/2} = 2.23$ nm. However, this gives only an average value of the cylinder radii, which does not tell anything about the radius distribution. The availability of the scattering curve in a wide q range allows one to fit the experimental results directly with relation 10.

The fit is obtained by visual comparison of the experimental to the theoretical curves. It is worth emphasizing that the range of radii from which the experimental curve can be fitted is very narrow. As a matter of fact, in the Kratky representation, the initial slope, the position of the maximum of the intensity, and the "width" of this maximum impose very severe conditions upon the set of values to be selected.

In the present cases, neither a monodisperse distribution using the radius derived from the Porod plot (see, for instance, Figure 4) nor any continuous distribution is appropriate to achieve the theoretical fits. Alternatively, the experimental results can be satisfactorily accounted for by considering a two-radii population (see Figures 4–7). It is worth noting that the agreement is not so satisfying at larger q vectors for 70 and 92 °C. This point will be commented on in due course. The radii together with their corresponding weight fractions are gathered in Table 1.

The approach with a two-radius population, although simple, is in good agreement with the mean cylinder radii as derived from the Porod plot. Perusal of Table 2 shows that the values of $\langle r_H^2\rangle$ derived from the Porod plot are close to those calculated from relation 12 with the couples of values of r_{Hi} and w_i by further assuming μ_{Li} to be directly proportional to r_{Hi}^2. Only the fit in the whole q range is thus liable to highlight the presence of a two-radius population. The fact that very good agreement is obtained

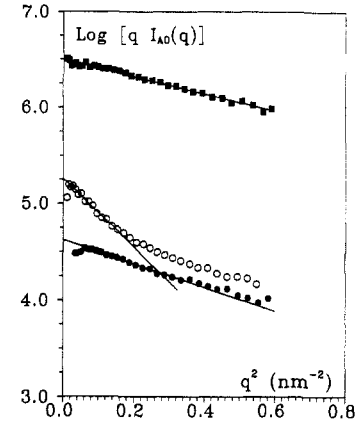

Figure 3. Porod plot ($\log[qI(q)]$ vs q^2) for (■) 17% bromobenzene gel, (●) 3% bromobenzene solution at 45 °C, and (○) 3% o-xylene solution at 86 °C.

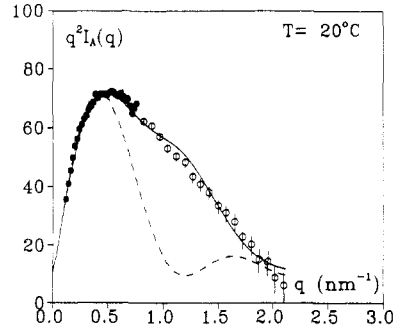

Figure 4. Kratky plot ($q^2I(q)$ vs q) for a 3% gel in bromobenzene at 20 °C. The solid line stands for the best fit with a two-radius population, and the dashed line stands for the calculation with one radius, i.e., the value derived from the Porod plot (see text). The two different symbols correspond to two different detector–sample distances.

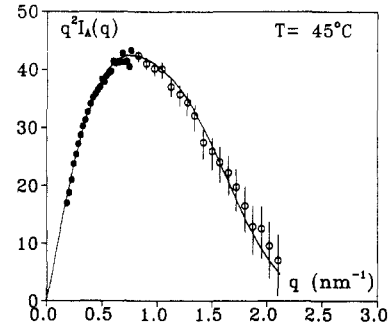

Figure 5. Kratky plot ($q^2I(q)$ vs q) for a 3% solution in bromobenzene at 45 °C. The solid line stands for the best fit (see text). The two different symbols correspond to two different detector–sample distances.

Table 1. Couples of Radii and Their Corresponding Weight Fractions Used in the Fit of the Experimental Data with Relation 10 by Considering a Two-Population Distribution

bromobenzene					
3%				17%	*o*-xylene 3%
20 °C	45 °C	70 °C	92 °C	20 °C	86 °C
$r_1 = 1.7 \pm 0.1$	$r_1 = 1.5 \pm 0.1$	$r_1 = 1.5 \pm 0.1$	$r_1 = 1.5 \pm 0.1$	$r_1 = 1.4 \pm 0.1$	$r_1 = 1.4 \pm 0.1$
$w_1 = 0.82$	$w_1 = 0.93$	$w_1 = 0.94$	$w_1 = 0.95$	$w_1 = 0.95$	$w_1 = 0.89$
$r_2 = 4.0 \pm 0.3$	$r_2 = 3.5 \pm 0.3$	$r_2 = 3.5 \pm 0.3$	$r_2 = 3.5 \pm 0.3$	$r_2 = 3.3 \pm 0.3$	$r_2 = 4.0 \pm 0.4$
$w_2 = 0.18$	$w_2 = 0.07$	$w_2 = 0.06$	$w_2 = 0.05$	$w_2 = 0.05$	$w_2 = 0.11$

Table 2. Different Parameters Derived from the Experimental Neutron Scattering Curves[a]

	bromobenzene					
	3%				17%	*o*-xylene 3%
	20 °C	45 °C	70 °C	92 °C	20 °C	86 °C
$\langle r_H^2 \rangle^{1/2}$ (nm) (1)	3.2 ± 0.3	2.2 ± 0.2	2.2 ± 0.2	2.1 ± 0.2	1.9 ± 0.1	3.8 ± 0.3
$\langle r_H^2 \rangle^{1/2}$ (nm) (2)	3.2	2.3	2.2	2.1	2.0	3.0
$\langle \mu_L \rangle_w$ (g/(mol nm))	2090 ± 125	1025 ± 60	990 ± 60	924 ± 60	968 ± 60	2010 ± 150
ρ_H (g/(nm^3 mol))	127 ± 13	110 ± 11	110 ± 11	107 ± 11	128 ± 13	183 ± 20

[a] 1 = radius determined from a Porod plot; 2 = radius calculated from relation 12 by using the couples of radii determined by a fit of the whole scattering curve with relation 10. $\langle \mu_L \rangle_w$ is the weight-averaged mass per unit length, and ρ_H is the experimental helix density.

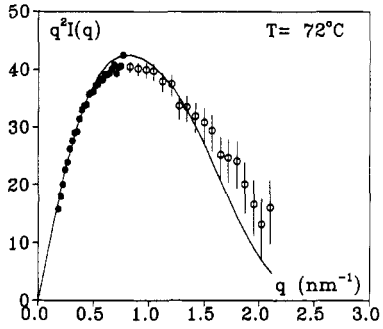

Figure 6. Kratky plot ($q^2I(q)$ vs q) for a 3% solution in bromobenzene at 72 °C. The solid line stands for the best fit (see text). The two different symbols correspond to two different detector–sample distances.

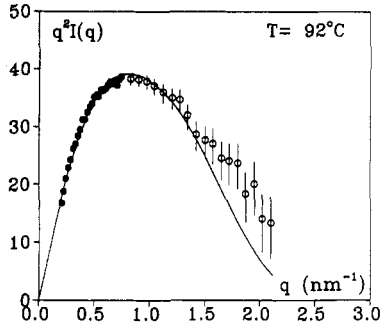

Figure 7. Kratky plot ($q^2I(q)$ vs q) for a 3% solution in bromobenzene at 92 °C. The solid line stands for the best fit (see text). The two different symbols correspond to two different detector–sample distances.

through the assumption of direct proportionality between μ_{Li} and r_{Hi}^2 further suggests that the high-radius cylinders consist of a discrete number of aggregated small-radius cylinders. The sketch of Figure 8 portrays a *bunch-like model* in which a gel junction is made up of several fibrils.

The model presented in Figure 8 differs drastically from our earlier model[8] in which the junctions were thought to be disorganized (*flail-like model*). The *flail-like model* cannot account straightforwardly for the significant increase of the second population of cylinders after gelation has set in while the *bunch-like model* can quite naturally.

The consequences of the above conclusions are that fiber-like structures already exist above the gelation point. It has already been proposed for PMMA[12,13] that helix formation precedes helix aggregation, unlike what usually

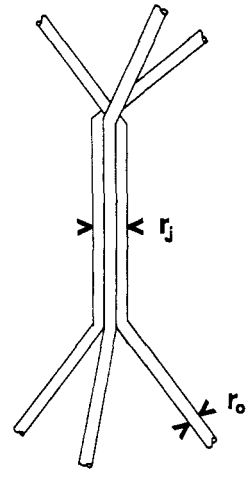

Figure 8. Schematic model of an organized junction composed of the merging of three basic fibrils (*bunchlike model*).

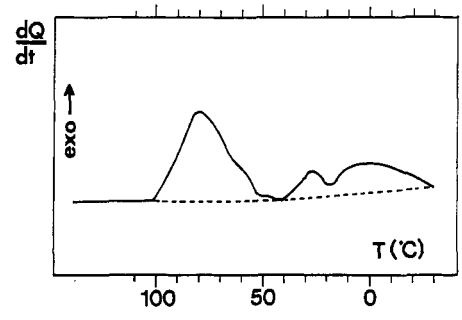

Figure 9. DSC trace obtained on cooling a 3% bromobenzene solution from 150 °C down to −30 °C at a rate of 0.25 °C/min.

happens in crystallizable polymers where both processes are concurrent. The thermal behavior recorded on cooling (see Figure 9) is consistent with this statement. As a matter of fact, three thermal events (exothermic) can be distinguished: one starting at about 100 °C and finishing at about 50 °C, one peaking at about 27 °C, and the last one at about 0 °C. As no gel occurs above 50 °C, it is assumed that the first exotherm corresponds chiefly to helix formation, while the exotherms below correspond to gelation. It is worth noting that at 92 and 70 °C helix formation has not reached completion whereas it is supposed to have at 45 °C. This may explain why the fits show significant discrepancy at larger q vectors with 92 and 70 °C samples: the presence of flexible chains gives

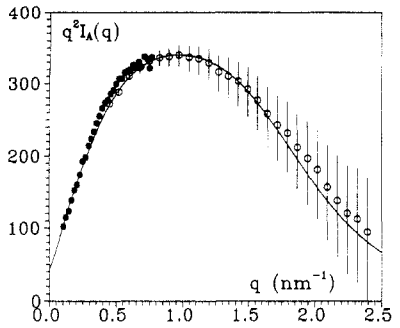

Figure 10. Kratky plot ($q^2I(q)$ vs q) for a 17% bromobenzene gel prepared by a quench at 0 °C. The two different symbols correspond to two different detector–sample distances.

an additional signal which decays less steeply than the one given by cylinders for this particular q range. Conversely, at 45 °C the amount of remaining flexible chains is negligible so that the scattered intensity is well-fitted with cylinder models only.

Before we review what types of helices are possibly involved, results obtained on the 17% gel are given and discussed. This gel was prepared by a quench at 20 °C. As with the other systems, a two-radius population of cylinders can be used to fit the data (see Figure 10 and Table 1).

Interestingly enough, the weight fraction of high-radius cylinders, that is, of junctions in the frame of the above model, is significantly lower than the one observed for the 3% gel. As the 17% gel is more concentrated, the number of junctions per unit volume is, however, still higher than in the 3% gel—hence the nonnegligible constant term in $q^2I_A(q)$. Nevertheless, the low weight fraction of junctions may seem paradoxical, as one would expect the same or nearly the same weight fraction of junctions independent of polymer concentration. As a matter of course, the weight fraction of junctions is similar to a degree of crystallinity which usually does not decrease when polymer concentration increases. To throw some light on the actual situation, it is worth recalling previous results[7,8] obtained on the same gel prior to and after swelling to equilibrium. It had been shown that the intensity scattered by a 17% gel as-prepared could be fitted with only one radius[22] whereas the intensity scattered by the same gel, once swollen to equilibrium, needed two radii in quite similar proportions to those derived here for the 3% gel. In the frame of the above model, this should imply formation of new junctions after swelling, which might appear somewhat paradoxical. The fact that mechanical properties are unexpectedly enhanced after swelling suggests a similar conclusion. The enhancement of mechanical properties is illustrated through the variation of the elastic modulus, E, with the polymer concentration, C_p (g/cm^3):[8]

$$\text{as-prepared gel} \quad E = 2.08 \times 10^2 C_p^{1.86} \text{ kPa}$$

$$\text{swollen gel} \quad E = 1.94 \times 10^3 C_p^{1.99} \text{ kPa}$$

These data show that, once the gel is swollen, although the polymer concentration has subsequently decreased, the modulus is larger than that of the original gel: for a 17% gel, E = 7.7 kPa vs 16.5 kPa after swelling (new C_p = 0.0924 g/cm^3).

The mechanism depicted in Figure 11 may account for the observed behavior. At high concentrations it is assumed that junction formation is impeded, for some reasons we shall not discuss here, so that the system resembles locally a heap of disordered logs, which may be

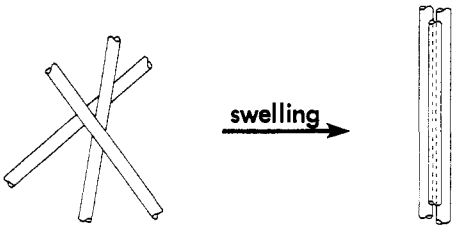

Figure 11. Sketch showing how a proto-junction transforms into an effective junction. This schematically illustrates how rods with larger diameters can appear on gel swelling.

designated as *proto-junctions*. While these proto-junctions can act as temporary knots, thus contributing to the gel modulus, they are thought to be highly labile compared to organized junctions. This is consistent with relaxation experiments carried out on the same gels that show a more rapid relaxation in nonswollen gels than in swollen gels.

On swelling, more room for chain rearrangement is available so that the "logs" of the proto-junctions can eventually align, thus forming additional organized junctions. This mechanism can account for the appearance of new junctions and, correspondingly, for the presence of additional high-radius cylinders in 17% gels once swollen to equilibrium.

As was already discussed elsewhere,[8] the presence of a large weight fraction of junctions in the 3% gels arises most probably from the preparation near the critical gel concentration ($2\% < C_{gel} < 3\%$). Under these conditions, unlike the 17% gels, 3% gels are already in a state close to swelling equilibrium.

In view of the sample's tacticity, the type of helix involved deserves to be discussed. The formation of a iPMMA/sPMMA stereocomplex has to be contemplated in this case.[3] Indeed, the low syndiotactic content makes it unlikely that helices of syndiotactic sequences, such as those described by Kusuyama et al.,[17] can be formed. This stereocomplex gives rise to the formation of a double helix where 18 sPMMA monomer units coil around 9 iPMMA monomer units. The pitch of this helix determined by Challa and Schomaker[6] has been found to be 1.84 nm and its external radius r_H = 1.2 nm. Its mass per unit length is therefore μ_L = 1470 g/(mol nm).

Scattering by helices of infinite length and of external radius r_H is given by the relation derived by Pringle and Schmidt:[18]

$$I(q) \sim (\pi\mu_L/q) \sum_{n=0}^{\infty} \epsilon_n \cos^2(n\phi/2) \frac{\sin^2(n\omega/2)}{(n\omega/2)^2} g_n^2(qr_H) \quad (13)$$

in which ω and ϕ are related to the helix cross-section, ϵ_0 = 1, ϵ_n = 2 for $n \geq 1$, and

$$g_n(qr_H) = \frac{2}{r_H^2} \int_0^{r_H} r J_n[qr\,(1 - a_n^2)^{1/2}]\, dr \quad (14)$$

in which J_n is the Bessel function of the first kind and order n and with the following conditions on the a_n terms dependent on the pitch of the helix P:

$$a_n = 2\pi n/qP \quad \text{for } q > 2\pi n/P$$

$$a_n = 1 \quad \text{for } q \leq 2\pi n/P$$

Here, if P = 1.84 nm, then, in the investigated q range, $a_0 = 0$ and $a_n = 1$ for $n > 1$ so that only the term for n = 0 remains. The terms containing ω and ϕ both equal 1. Under these conditions eq 14 reduces to the well-known

form,[19] which appears in relation 10:

$$I(q) \sim (\pi\mu_L/q)\left[\frac{2J_1(qr_H)}{qr_H}\right]^2 \quad (15)$$

Consequently, the use of relation 10 is perfectly legitimate in the present case in the investigated q range.

The value of 1.5 nm found experimentally is therefore rather consistent with this type of helical form. This is the more so if one bears in mind that for such a tacticity the helical arrangement is liable to contain defects so that the theoretical radius of 1.2 nm is not expected to be strictly observed.

However, when it comes to comparing the mass per unit length $\langle\mu\rangle_w$ found experimentally to the theoretical one, the discrepancy cannot be overlooked. This parameter is calculated either from the initial slope in the Kratky plot

$$q^2I_A(q) - \text{const} = C_p\pi q\sum_i w_i\mu_{Li} = C_p\pi q\,\langle\mu_L\rangle_w \quad (16)$$

or from the intercept in the Porod plot (see relation 11).

In Table 2 are gathered the values of the mass per unit length for each sample. As can be seen, this parameter is, in most cases, lower than the theoretical one, something which was already reported in a previous publication.[7] However, $\langle\mu_L\rangle_w$ is not suited for further discussion as it depends upon the amount of high-radius cylinders. A relevant parameter is the *helix density*, ρ_H, which reads

$$\rho_H = \frac{\langle\mu_L\rangle_w}{\pi\sum_i w_i r_{Hi}^2} \quad (17)$$

As can be seen from inspection of Table 2, ρ_H is virtually the same independent of temperature, namely, ρ_H = 118 ± 10 g/(mol nm^3), but is about 3 times lower than the theoretical value (ρ_H = 325 g/(mol nm^3)). The presence of defects along the helical form is not expected to lower the theoretical value to the required extent. In ref 7, Fazel et al. suggested that complexation by the solvent of the stereocomplex helix may be envisaged. This assumption further relies on various observations:[17] crystallization from the bulk only occurs on submitting the sample to solvent vapor, and removal of the solvent usually leads to the disappearance of the organized structure.

If a polymer–solvent complex is formed, then it is likely that the calculated contrast factor, A^2, is overestimated and, correspondingly, the absolute scattered intensity underestimated. What follows is not an attempt to demonstrate the existence of such a complex but simply an attempt to show that such a working hypothesis is not contradictory to the neutron data. For a complex, the scattering amplitude should read

$$A_c^2 = \left(b_c - \frac{v_c}{v_s}b_s\right)^2 = \left(b_p + nb_s - \frac{\lambda(v_p + nv_s)}{v_s}b_s\right)^2 \quad (18)$$

in which b_p and b_s are the scattering amplitudes of the polymer and the solvent, respectively, v_p and v_s are their molar volumes, n is the number of solvent molecules per monomer unit in the complex, and λ is a factor which takes into account the effect of complexation to determine the molar volume of the complex. For λ = 1 there is no complexation as the molar volumes would be simply additive. It is worth noting that the concentration, C_c, and the molar mass, m_c, to be taken should be those of the complex to calculate K and ultimately the absolute intensity. However, it can be shown that, in dilute systems,

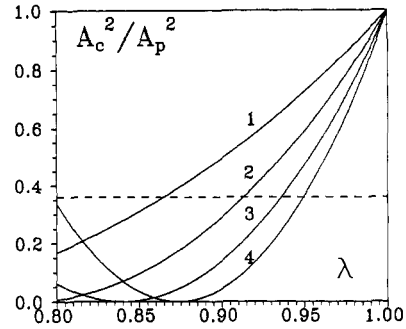

Figure 12. Theoretical ratio of the scattering amplitude by a polymer–solvent complex form over the amplitude calculated for the polymer in the noncomplexed form as a function of λ (see text). Numbers stand for the number of solvent molecules per monomer.

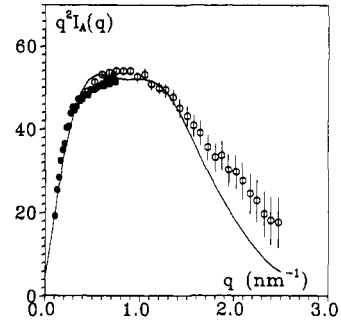

Figure 13. Kratky plot ($q^2I(q)$ vs q) for a 3% o-xylene solution at 86 °C. The two different symbols correspond to two different detector–sample distances. The solid line stands for the best fit (see text).

the ratio $C_c\mu_{Lc}/m_c^2 \simeq C_p\mu_{L0}/m_p^2$, μ_{L0} being the partial mass per unit length of the polymer in the complex. As a result, the only parameters worth examining remain the *scattering amplitude* vs the *helix density*, that is, to find out which scattering amplitude gives the correct polymer helix density. It is convenient to plot the ratio of the scattering amplitude of the complex given by relation 18 to that calculated for the polymer in the absence of complexation as a function of λ with n as a parameter (Figure 12). The correct ratio can be obtained without too much drastic conditions on the resulting molar volume. For n = 2 the complex molar volume needs to be only 9% smaller than simple additivity. As the solvent molecules are likely to be housed within the cavities created by the PMMA side groups,[20] such values of λ are not unreasonable.

Finally, it is worth noting that the theoretical *helix density*, once expressed in g/cm^3, gives 0.54 g/cm^3. If the stereocomplex were organized without intercalated solvent, that is, helices organizing parallel to one another, then the resulting material would possess a density much too low compared to the usual density of PMMA (≈1.2 g/cm^3), or even as usual polymeric materials. The intercalation of solvent, i.e., formation of a polymer–solvent complex, can resolve this density anomaly.

(2) PMMA/*o*-Xylene Gels and Aggregates. A 3% o-xylene solution was quenched from 145 °C to 86 °C, at which temperature the resulting solution was studied. The results are presented in Figure 13 by means of a Kratky representation. The plot of Figure 13 is reminiscent of what was obtained with bromobenzene at 92 and 72 °C. A fit can be achieved by considering again a two-radius population. The radii are of the same order of magnitude as with bromobenzene (1.4 and 4.0 nm). Also, a noticeable discrepancy appears in the high-q range, which, as with bromobenzene, suggests the presence of flexible chains. The mean radius derived from the Porod plot (see Figure

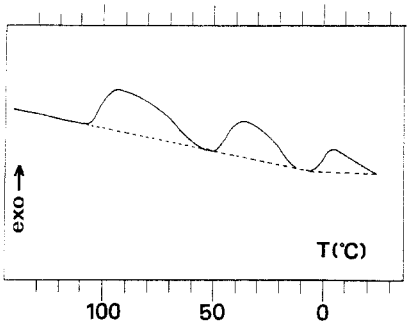

Figure 14. DSC trace of a 3% *o*-xylene solution cooled from 145 °C down to −25 °C at a rate of 0.25 °C/min.

3 and Table 2) is, however, larger than the one calculated from the radii derived from the fit (3.8 vs 3.0 nm). Clearly, the fit is not as satisfying as what was achieved with bromobenzene gels. We had already reported that PMMA/*o*-xylene gels are less homogeneous that their counterparts in bromobenzene. Description of PMMA/*o*-xylene gels and aggregates with a two-population distribution is evidently a naive view of the actual molecular structure. However imperfect, this fit reveals the presence of the same basic rod-like structure, which is most probably the stereocomplex double helix.

The thermal behavior resembles the one observed in bromobenzene (see Figure 14). In particular, there is a high-temperature exotherm, which probably represents the coil–helix transition. However, the fit indicates that the amount of junctions is significantly larger in *o*-xylene than it is for bromobenzene in this domain of temperature. While the coil–helix transition probably occurs first, it becomes rapidly concurrent with helix aggregation. In *o*-xylene both processes may not be as distinct as in bromobenzene.

The *helix density* is higher in the case of *o*-xylene (see Table 2). This may suggest a lower degree of solvation. Unlike bromobenzene, which, due to the bromine atom, is liable to interact better with PMMA, *o*-xylene is not liable to be housed within the cavities created by the ester groups. Consequently, the degree of solvation should be lower, which is consistent with the experimental *helix density* found here.

Concluding Remarks

Results presented in this paper are again consistent with the existence of a basic rod-like structure of cross-sectional radius 1.5 ± 0.1 nm, which can be observed in two different solvents, bromobenzene and *o*-xylene. The analysis of the results can be achieved by considering the double-helical structure arising from stereocomplexation of iPMMA sequences by sPMMA ones. To account for the corresponding defect of mass per unit length, complexation of the helical structure by the solvent is contemplated. Future investigations to be carried out on these systems should focus on the direct demonstration of the occurrence of a polymer–solvent complex.

The analysis of the present data has allowed us to settle the question of the nature of the junctions, i.e., disorganized (*flail-like model*) or organized (*bunch-like model*). The latter model can quite simply explain consistently both the neutron data and the rheological properties.

Finally, the SANS results together with the thermal analysis again give additional support to the two-step mechanism of gel formation: *helix formation* and then *helix aggregation*. It seems that this mechanism predominates in the formation of thermoreversible gels.[21]

References and Notes

(1) Spěvaček, J.; Schneider, B. *Makromol. Chem.* **1974**, *175*, 2939.
(2) Spěvaček, J.; Schneider, B. *Makromol. Chem.* **1975**, *176*, 729.
(3) Spěvaček, J.; Schneider, B. *Adv. Colloid Interface Sci.* **1987**, *27*, 81.
(4) Bosscher, F.; ten Brinke, G.; Challa, G. *Macromolecules* **1982**, *15*, 1442.
(5) Spěvaček, J. *Makromol. Chem., Macromol. Symp.* **1990**, *39*, 71.
(6) Schomaker, E.; Challa, G. *Macromolecules* **1989**, *22*, 3337.
(7) Fazel, N.; Fazel, Z.; Brûlet, A.; Guenet, J.-M. *J. Phys. II* **1992**, *2*, 1617.
(8) Fazel, Z.; Fazel, N.; Guenet, J.-M. *J. Phys. II* **1992**, *2*, 1745.
(9) Schomaker, E.; Challa, G. *Macromolecules* **1988**, *21*, 2195.
(10) Schomaker, E.; Challa, G. *Macromolecules* **1988**, *21*, 2203.
(11) Guenet, J.-M.; Rochas, C.; Brûlet, A. *J. Phys. IV* **1994**, *3 C8*, 99.
(12) Sedlaček, B.; Spěvaček, J.; Mrkvickova, L.; Stejskal, J.; Horska, J.; Baldrian, J.; Quadrat, O. *Macromolecules* **1984**, *17*, 825.
(13) Berghmans, H.; Donkers, A.; Frenay, L.; De Schryver, F. C.; Moldanaers, P.; Mewis, J. *Polymer* **1987**, *28*, 97.
(14) *Introduction à la spectrométrie neutronique*, CEN Saclay, 1974.
(15) Ragnetti, D.; Oberthür, R. *Colloid Polym. Sci.* **1986**, *264*, 32.
(16) Cotton, J. P. In *Neutron, X-ray and Light Scattering*; Lindner, P., Zemb, T., Eds.; Elsevier: Amsterdam, 1991.
(17) Kusuyama, H.; Miyamoto, N.; Chatani, Y.; Tadokoro, H. *Polym. Commun.* **1983**, *24*, 119.
(18) Pringle, O. A.; Schmidt, P. W. *J. Appl. Crystallogr.* **1971**, *4*, 290.
(19) Porod, G. *Acta Phys. Aust.* **1948**, *2*, 255.
(20) Klein, M.; Guenet, J.-M. *Macromolecules* **1989**, *22*, 3716.
(21) See, for example: Guenet, J.-M. *Thermoreversible Gelation of Polymers and Biopolymers*; Academic Press: London, 1992.
(22) For the results presented in ref 8, only one radius was necessary for the fit, probably because the *q* range was not as extended as here and also because the fraction of high radius is noticeably low.